Analysis of the damping factor in phase-shift migration

Daniel Rosales[1]

ABSTRACT

Cosmetic processes, the use of different parameters in standard seismic data processing in order to improve the appearance of the data, are generally not considered in the mathematical formulation of migration algorithms, even though they are physically and mathematically related to the wave propagation process. The inclusion of causality and viscosity in phase-shift migration as a damping factor will take care of these "superficial" features and numerical instability due to evanescent energy.

INTRODUCTION

Phase shift migration uses the dispersion relation of the scalar wave equation (Gazdag, 1978) in order to perform wavefield downward continuation. This relation presents computational implementation problems when facing evanescent waves due to negative number in the square root. The solution is to redefine the Fourier kernel for the downward continuation by adding a damping factor, ϵ, (Claerbout, 1999a). However, this redefinition faces stability problems related to the choice of ϵ.

Concepts like causality (Claerbout, 1999b) and viscosity (van Trier and Symes, 1990; Claerbout, 1995) can be incorporated in the redefinition of the Fourier kernel in order to perform phase shift migration. This modification does not discard the evanescent energy in the computational implementation of phase shift migration; it is steady with respect to the damping factor, and it incorporates *cosmetic* features to the final image.

This work presents a review of the theory for the damping factor in the dispersion relation. Numerical examples show how the omission of causality and viscosity in the redefinition of the dispersion relation translates into a loss of high frequency information in the final migration result. Finally, I will show examples with the redefinition of the dispersion relation that incorporates causality and viscosity in phase-shift migration.

THEORY REVIEW

Migration is the process of downward continuation of the wavefield plus the application of the imaging condition ($t = 0$). The downward continuation process can be achieved in the

[1]**email:** daniel@sep.stanford.edu

Fourier domain (Stolt, 1978; Gazdag, 1978). The phase-shift method extrapolates the wavefield downwards with $\exp(ik_z z)$, where the *dispersion relation of the scalar wave equation* defines k_z (Claerbout, 1985):

$$\begin{aligned} k_x^2 + k_z^2 &= \frac{\omega^2}{v^2}, \\ k_z &= \pm\sqrt{\frac{\omega^2}{v^2} - k_x^2}. \end{aligned} \tag{1}$$

The use of (1) for calculating k_z obscures two aspects of it: first, which of the two square roots is intended, and second, what happens when $k_x^2 > \frac{\omega^2}{v^2}$ (evanescent waves). Claerbout (1999a) emphasizes the fact that for coding and theoretical work it is necessary to define k_z for both positive and negative ω, and for all k_x values.

The inclusion of the damping factor can solve the ambiguity in the k_z selection. This damping is traditionally included as a cutoff frequency; Claerbout (1999a) defines a function $R = ik_z(\omega, k_x)$ that includes this cutoff frequency as:

$$R = ik_z = \sqrt{(-i\omega + \epsilon)^2 + (vk_x)^2}. \tag{2}$$

This function (2) has a positive real part (Figure 1), which implies that we can extrapolate waves safely with $e^{\pm Rz}$. However, since the damping factor has been included as a cutoff frequency we can lose frequency information with an inappropriate choice of ϵ.

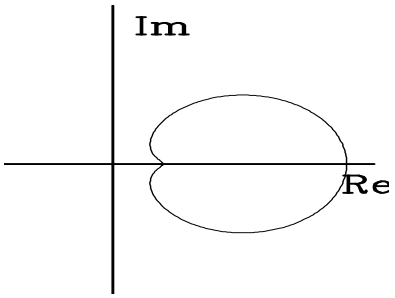

Figure 1: Function (2) for an $\epsilon = 0.1$. (Claerbout, 1999a) daniel1-fradan [ER]

A theoretical redefinition of $R = ik_z$ that incorporates causality and viscosity concepts will not only solve for the ambiguity of the k_z selection but also preserve the frequency content of our original data.

Redefining R

The principle of causality: no response before a stimulus, is not considered in the R definition [equation (2)]. The omission of causality translates into improper behavior of the high frequencies. In order to include causality into the definition of R, let $s = -i\hat{\omega}$ be the causal, positive, discrete representation of the differentiation operator,

$$s = -i\hat{\omega} = \frac{2}{\Delta t}\frac{1-\rho Z}{1+\rho Z}, \tag{3}$$

which is simplified by writting $s = -i\omega + \epsilon$. Claerbout (1985) proposes the use of the following Muir recursion starting from $R_0 = s$:

$$R_{n+1} = s + \frac{X^2}{s + R_n}. \tag{4}$$

This recursion produces a continuous fraction. Studying the limit for $n \to \infty$ we obtain:

$$\begin{aligned} R_\infty &= s + \frac{X^2}{s + R_\infty}, \\ R_\infty(s + R_\infty) &= s^2 + X^2 + s R_\infty, \\ R_\infty^2 &= s^2 + X^2, \\ R &= \pm\sqrt{s^2 + X^2}. \end{aligned} \tag{5}$$

If we let $X^2 = v^2 k_x^2$ in equation (5) then R is $\pm i k_z v$. The retarded time expression of $e^{-R\frac{z}{v}}$ [equation (6)] will downward continue, in time, the data for phase-shift migration.

$$e^{-R\frac{z}{v}} = e^{-(R-s)\frac{z}{v}} e^{-s\frac{z}{v}}. \tag{6}$$

The following change of variables:

$$R' = R - s \tag{7}$$

transforms the Muir recursion (4) into:

$$R'_{n+1} = \frac{v^2 k_x^2}{2s + R'_n}. \tag{8}$$

Again, taking the limit for $n \to \infty$ in this recursion we will obtain

$$\begin{aligned} R'_\infty \cdot (2s + R'_n) &= v^2 k_x^2 \\ {R'_\infty}^2 + 2s R'_\infty - v^2 k_x^2 &= 0 \end{aligned} \tag{9}$$

This quadratic expression yields to two square roots for R',

$$R' = -s \pm \sqrt{s^2 + v^2 k_x^2}. \tag{10}$$

We need to select the one that is able to handle the evanescent region, *i.e*, the square root that goes to zero at $k_x = 0$, which corresponds to the positive square root.

$$R' = -s + \sqrt{s^2 + v^2 k_x^2}, \tag{11}$$

multiplying numerator and denominator by $s + \sqrt{s^2 + v^2 k_x^2}$, equation (11) transforms into:

$$R' = \frac{v^2 k_x^2}{\sqrt{s^2 + v^2 k_x^2} + s}. \tag{12}$$

I already showed that the real part of $\sqrt{s^2+v^2k_x^2}$ is positive (Figure 1); therefore, R', as defined in equation (12), also has a positive real part.

Finally, we downward continue the data in the Fourier domain by multiplying by:

$$e^{-R'\frac{z}{v}}e^{-i\omega\frac{z}{v}} \tag{13}$$

Expression (13) incorporates the causality and viscosity concepts in phase shift migration, controls the evanescent energy and will not allow discontinuity between evanescent and non-evanescent regions.

Controlling the angle

It is possible to perform a dip filter with our phase-shift migration algorithm; because we calculate R' with the Muir recursion (4,8), we can use the recursion starting with $R_0 = r_0 s$, in order to have control on the desire dip.

$$R'_0 = s(r_0 - 1), \tag{14}$$

where r_0 defines the cosine of the angle that starts the Muir recurrence, often 0° or 45°; following the recursion (8) we find

$$R'_1 = \frac{v^2k_x^2}{s(1+r_0)} \tag{15}$$

and subsequently:

$$R'_2 = \frac{v^2k_x^2}{2s+\frac{v^2k_x^2}{s(1+r_0)}} \tag{16}$$

The expressions (14), (15), and (16) are the relations for a 5°, 15°, and 45° dip migration in the Fourier-domain, respectively.

NUMERICAL EXAMPLES

Figure 2 shows from left to right: a two-spike synthetic model, modeling with equations (1) and (2). It is possible to observe the decay of amplitude (energy) with respect to time when we include the damping factor (ϵ) in our modeling equation. The same effect is observable in Figure 3, which shows the migration results using the results of Figure 2.

The energy decay is a function of the damping factor (ϵ). Figure 4 presents experimental results of the energy variability with respect to ϵ. The experiment consists of modeling and migration of the two-spike model with equation (2) for different values of ϵ. Each sample in the plot (Figure 4) represents the energy of each modeling-migration result for ϵ ranging

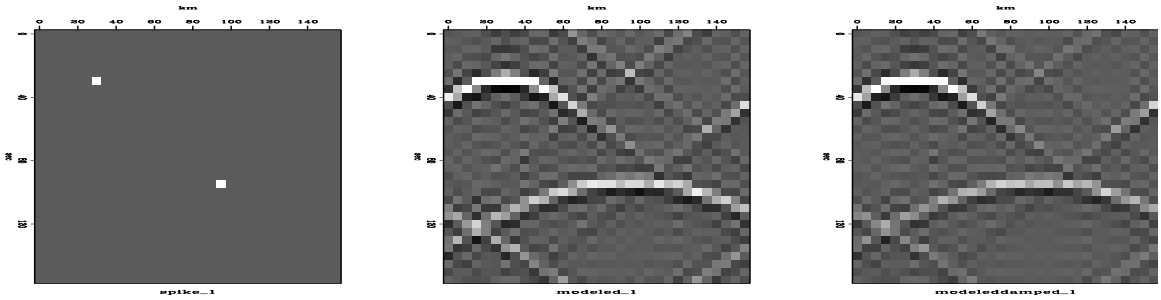

Figure 2: Modeling Comparison. From left to right: synthetic model; modeling with $k_z = \sqrt{\frac{\omega^2}{v^2} - {k_x}^2}$; modeling with $R = ik_z = \sqrt{(-i\omega+\epsilon)^2 + v{k_x}^2}$ daniel1-compar_1 [ER]

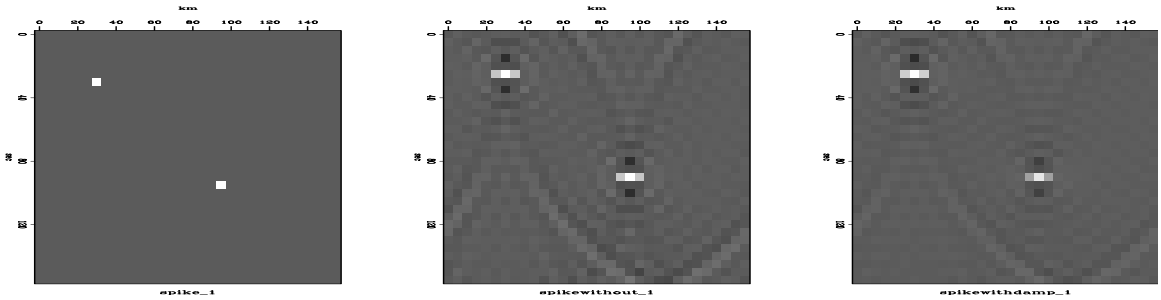

Figure 3: Modeling-Migration Comparison. From left to right: synthetic model; results with $k_z = \sqrt{\frac{\omega^2}{v^2} - {k_x}^2}$; results with $R = ik_z = \sqrt{(-i\omega+\epsilon)^2 + v{k_x}^2}$ daniel1-modmig_1 [ER]

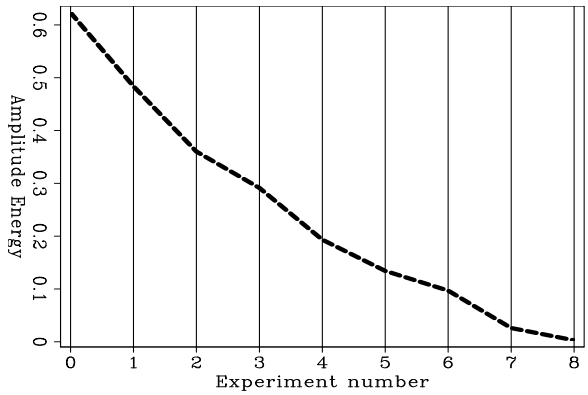

Figure 4: Energy decay with respect to the damping factor ϵ daniel1-energy [ER]

between 0.002 and 0.04 every 0.002. It is possible to observe that the energy decays exponentially with respect to the damping factor; this decrease is due to the omission of causality in the redefinition of ik_z.

For comparison, Figure 5 shows three results of the experimental procedure described before. It is possible to observe that the bigger the damping factor, the less energy is present in the final result.

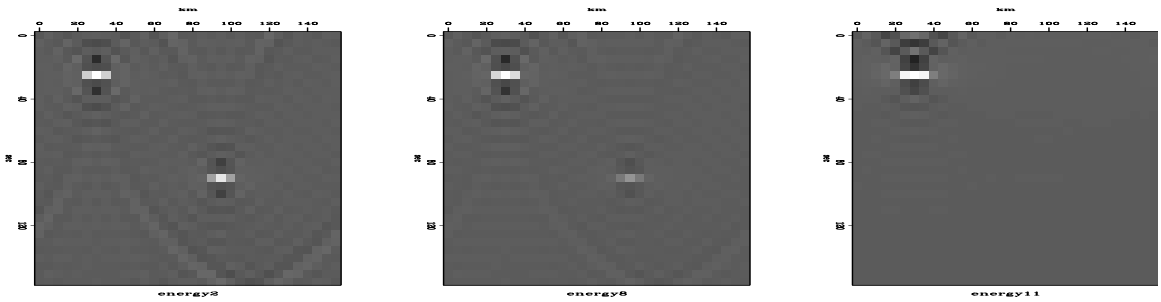

Figure 5: Three different values of ϵ for the original model, right with $\epsilon = 0.00312$, center $\epsilon = 0.008$, left $\epsilon = 0.04$ daniel1-threeep [ER]

The new R

Including causality and viscosity in the definition of $R = ik_z$ (equation 12) it is possible to preserve the energy content for any arbitrary ϵ value.

Figure 7 presents the modeling-migration results, using the model of synthetic data set in Figure 6, with equations (2) and (12) for two different values of ϵ. Figure 8 shows the respective frequency spectrum.

We can assure the stability of the R definition presented in equation (12) based on the results of Figures 7 and 8; besides, this R definition is valid for all values of ω and k_x.

We also perform the phase-shift migration over a real data set, we present the results on Figures 9 and 10. These results show a comparison between phase-shift migration without considering the damping factor [R definition in equation (1)] and considering the damping factor [R definition in equation (12)].

The image that we obtain with the damping factor is much cleaner than the image without the damping factor; therefore, the events definition and the faults are more clear.

Angle results

In the previous section we discussed the possibility of controling the aperture angle in phase-shift migration. Here, we present some synthetic results that show how we can control the angle using the expressions in (15), (16), (12).

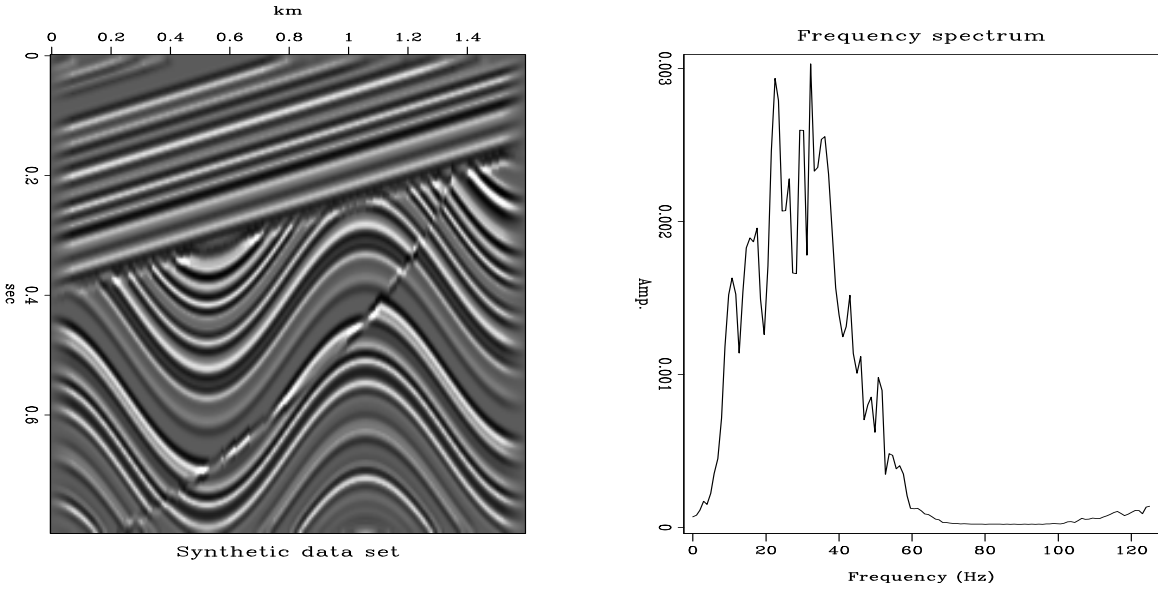

Figure 6: Synthetic data set daniel1-mod3 [ER]

Figure 11 shows the impulse response for the expressions (15), (16), (12). Observe how we limit the aperture angle response with the three different expressions.

CONCLUSIONS

We present a stable definition of $R = ik_z$ that includes the causality and viscosity concepts in phase-shift migration; moreover, this expression is valid for any value of ω and k_x.

We implemented the damping factor ϵ in the R definition, equation (12), such that there is no loss of high frequency information. This redefinition also presents the possibility of having different damping factors in order to improve even more the quality of the final image.

The fact that we use Muir recursion to develop a stable R definition lets us have control over the migration angle just as wavefield migration does.

REFERENCES

Claerbout, J. F., 1985, Imaging the earth's interior: Blackwell Scientific Publications.

Claerbout, J., 1995, The adjoint of the viscous wave equation: SEP–**89**, 191–200.

Claerbout, J. F., 1999a, Basic earth imaging: `http://sepwww.stanford.edu/sep/prof/index.html`.

Claerbout, J. F., 1999b, Fundamentals of geophysical data processing: `http://sepwww.stanford.edu/public/docs/fgdp/toc_html/index.html`.

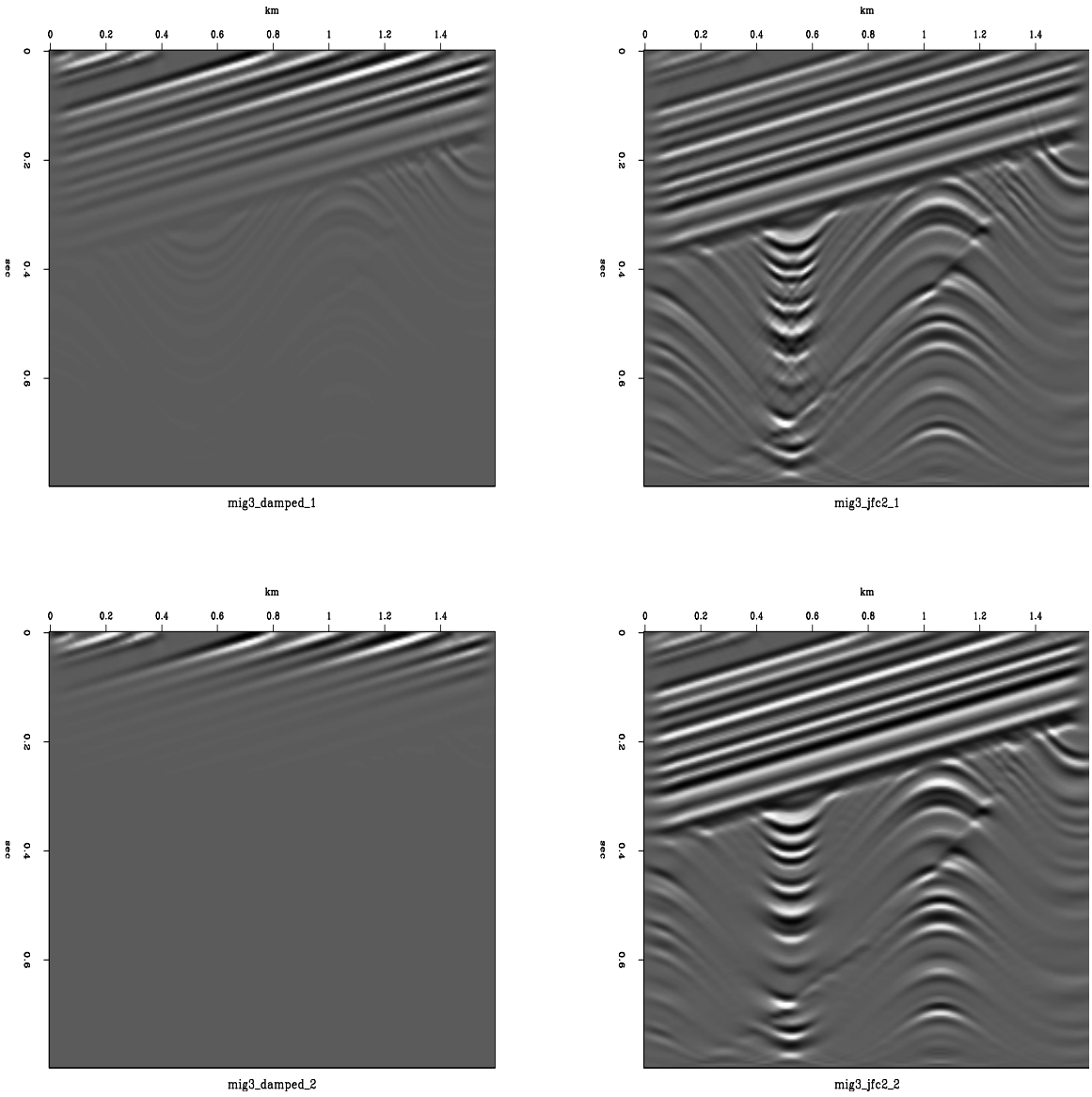

Figure 7: Comparison between modeling-migration using model on Figure 6 using R definition as in equation (2), left, and equation (12), right. The top figures have a damping factor $\epsilon = 5$, the bottom figures have a damping factor of $\epsilon = 15$ daniel1-mod3_comp [ER]

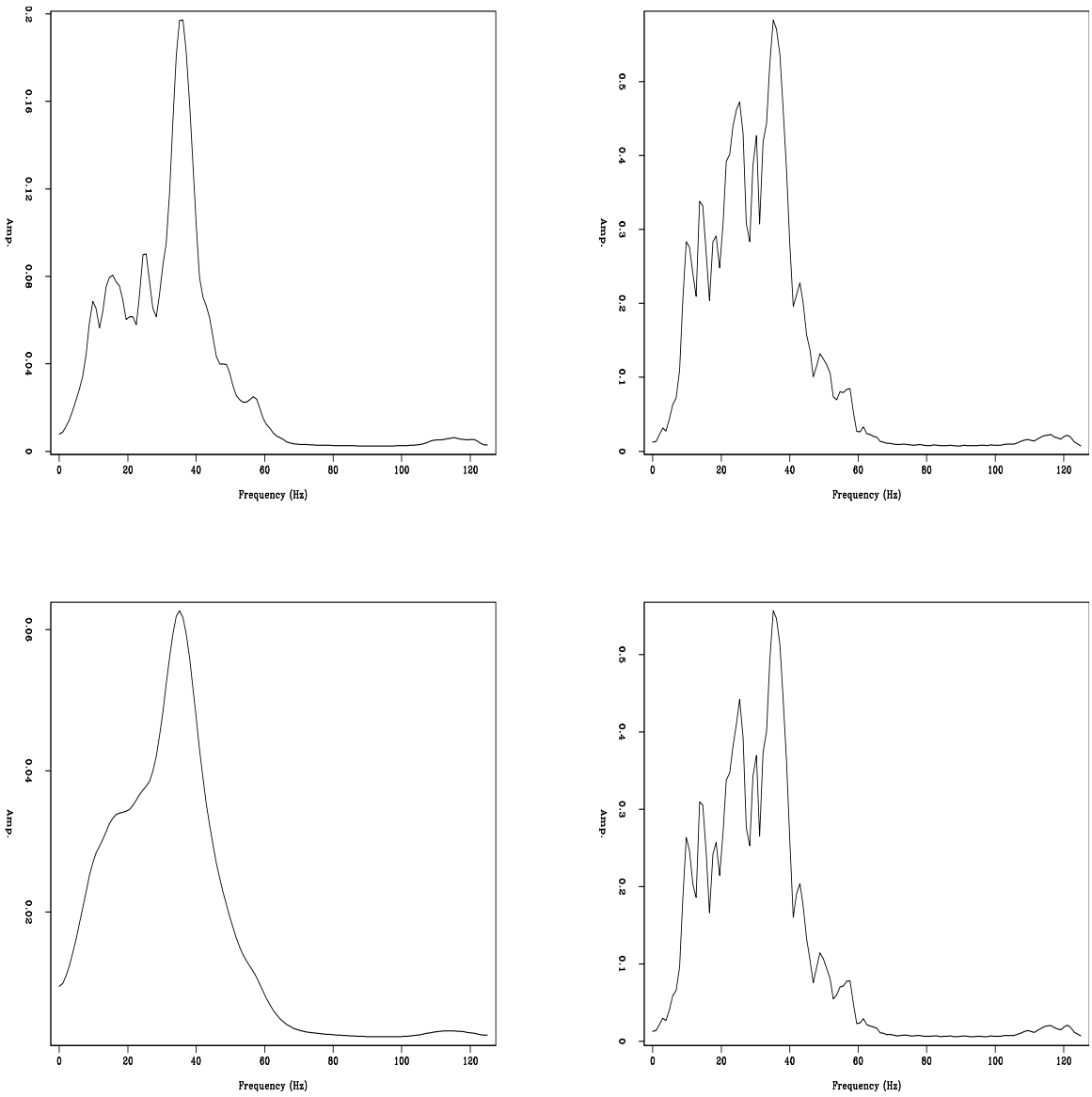

Figure 8: Comparison between the frequency spectrum of the modeling-migration results on Figure 7. The top figures have a damping factor $\epsilon = 5$, the bottom figures have a damping factor of $\epsilon = 15$ daniel1-mod3_freq [ER]

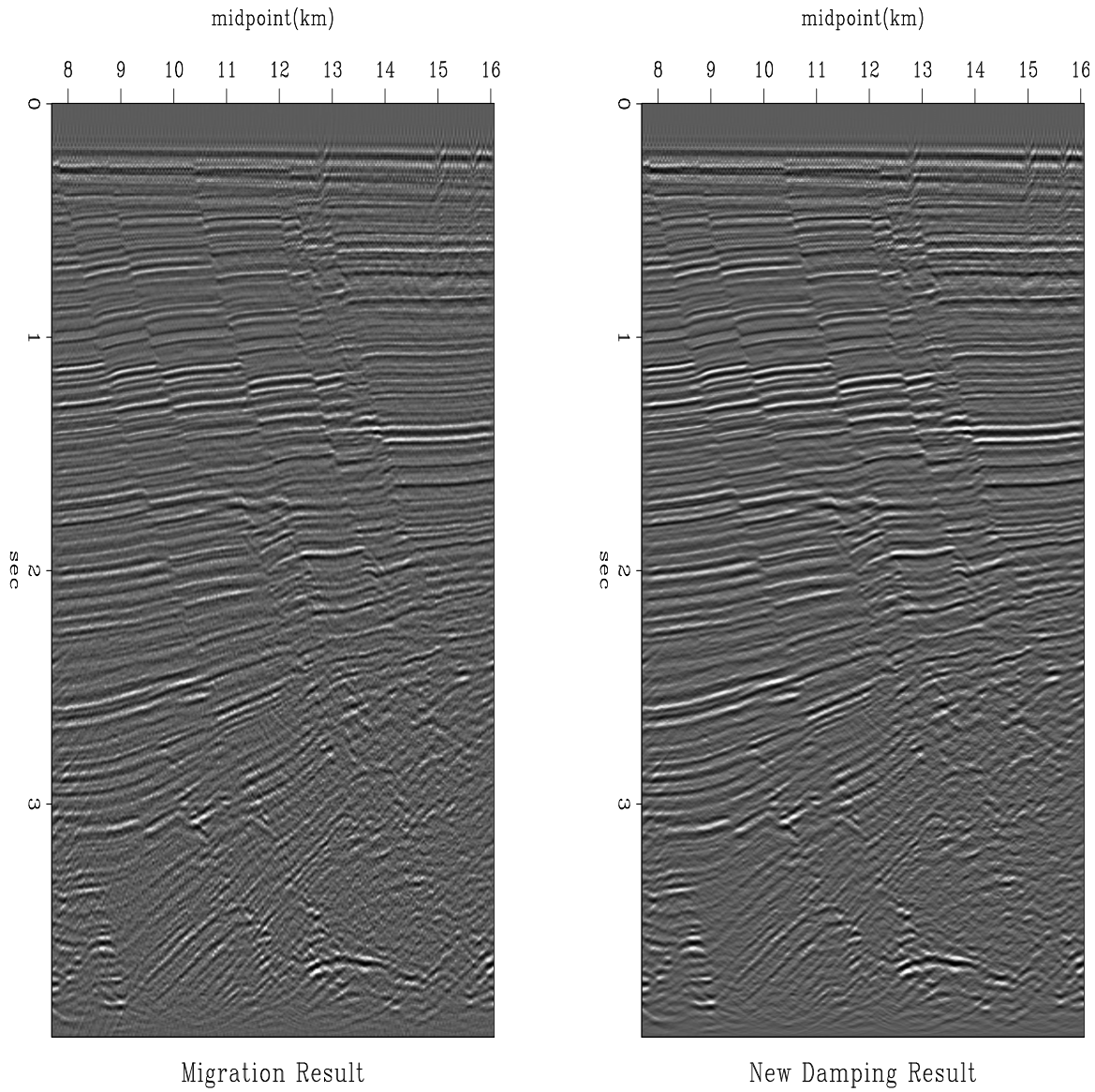

Figure 9: Data Comparison. Left the migration result without considering damping. Right the migration result using the new R with $\epsilon = 5$ daniel1-out1 [ER,M]

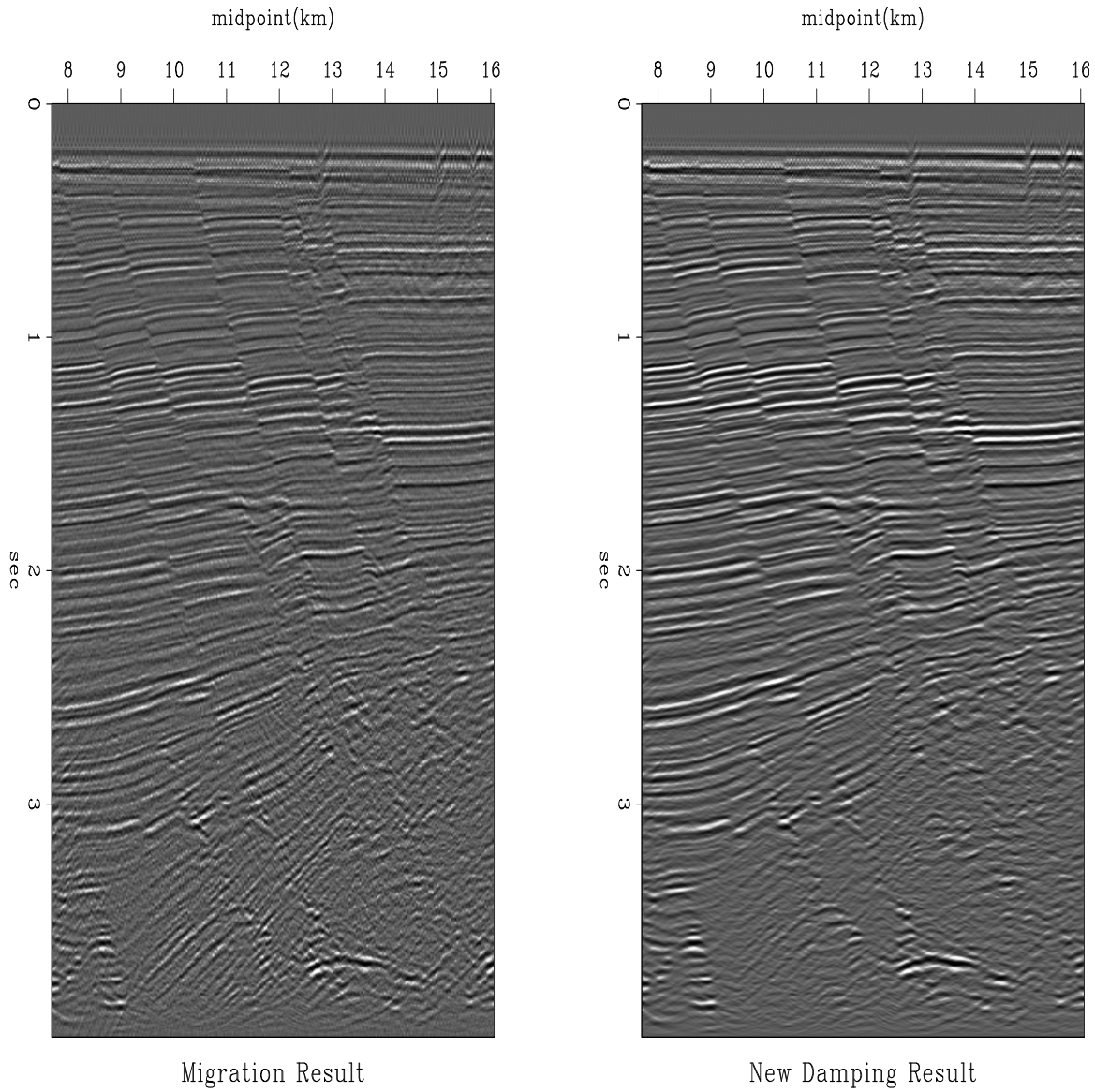

Figure 10: Data Comparison. Left the migration result without considering damping. Right the migration result using the new R with $\epsilon = 15$ daniel1-out2 [ER,M]

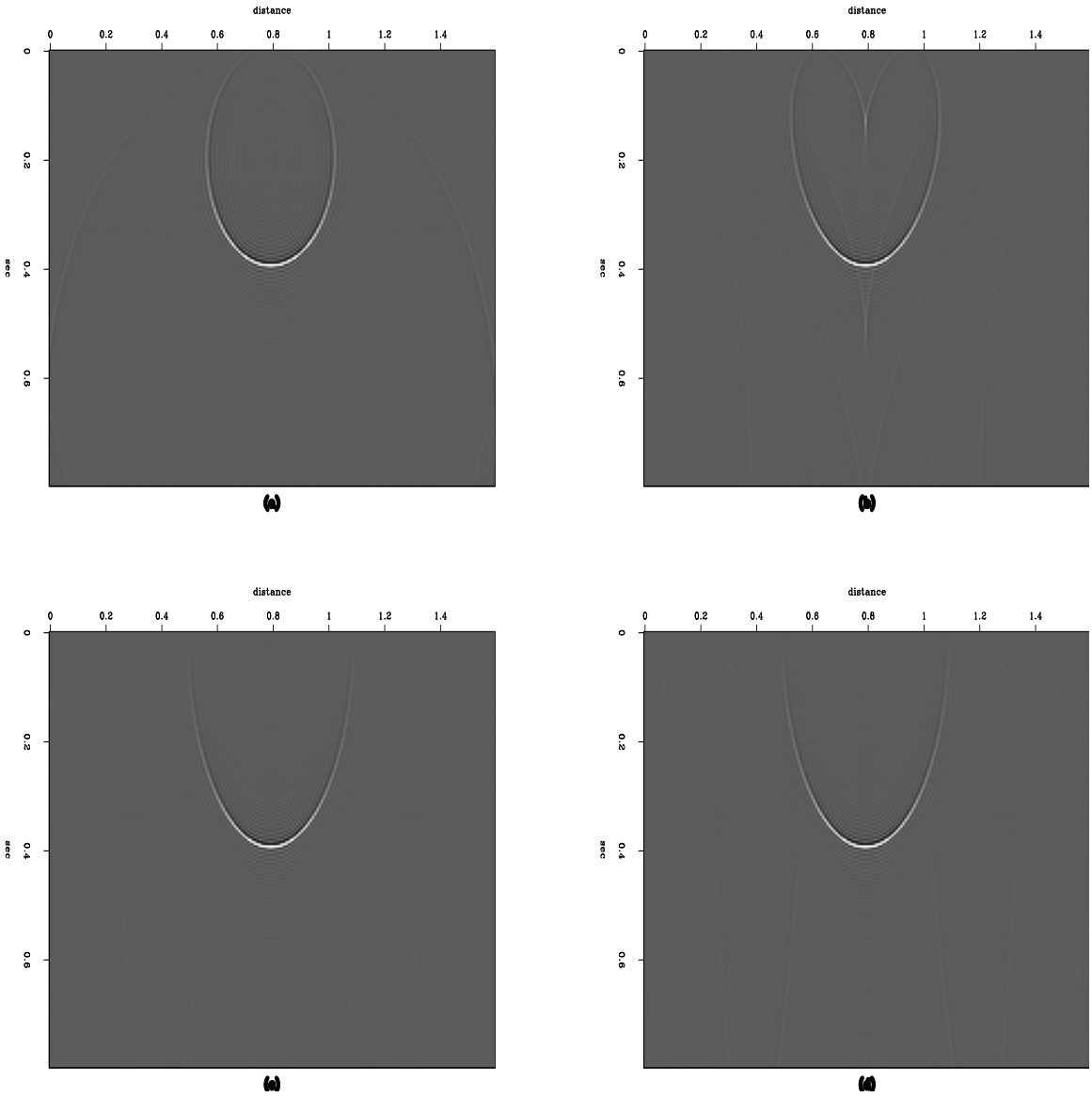

Figure 11: Angle control; the impulse responses correspond to, (a), (b), (c), and (d) corresponds to the the 15°, 45°, 90°, and the response from the double square root equation (1), respectively. daniel1-compan [ER]

Gazdag, J., 1978, Wave equation migration with the phase-shift method: Geophysics, **43**, no. 7, 1342–1351.

Stolt, R. H., 1978, Migration by Fourier transform: Geophysics, **43**, no. 1, 23–48.

van Trier, J., and Symes, W. W., 1990, Upwind finite difference calculation of traveltimes: SEP–**65**, 41–58.